Cryogenic Fracturing of Wellbores Under True Triaxial-Confining Stresses: Experimental Investigation

Minsu Cha, Texas A&M University; **Naif B. Alqahtani,** King Abdulaziz City for Science and Technology; **Bowen Yao** and **Xiaolong Yin,** Colorado School of Mines; **Timothy J. Kneafsey,** Lawrence Berkeley National Laboratory; and **Lei Wang, Yu-Shu Wu,** and **Jennifer L. Miskimins,** Colorado School of Mines

Summary

A laboratory study of cryogenic fracturing was performed to test its ability to improve oil/gas recovery from low-permeability reservoirs. Our objective is to develop well-stimulation technologies using cryogenic fluids [e.g., liquid nitrogen (LN)] to increase permeability in a large reservoir volume surrounding wells. The new technology has the potential to reduce formation damage caused by current stimulation methods and minimize or eliminate water usage.

The concept of cryogenic fracturing is that a sharp thermal gradient (thermal shock) created at the surfaces of formation rocks by applying cryogenic fluid can cause strong local tensile stress and start fractures. We developed a laboratory system for cryogenic fracturing under true-triaxial loading, with LN-delivery/control and -measurement systems. The loading system simulates confining stresses by independently loading each axis up to approximately 5,000 psi on 8×8×8-in. cubes. Temperature in boreholes and at block surfaces and fluid pressure in boreholes were continuously monitored. Acoustic and pressure-decay measurements were obtained before and at various stages of stimulations. Cubic blocks (8 × 8×8-in.) of Niobrara shale, concrete, and sandstones were tested, and stress levels and anisotropies varied. Three schemes were considered: gas fracturing without cryo-stimulation, gas fracturing after low-pressure cryogen flow-through, and gas fracturing after high-pressure cryogen flow-through.

Results from pressure-decay tests show that LN stimulation clearly increases permeability, and repeated stimulations further increase the permeability. Acoustic velocities and amplitudes decreased significantly after cryo-stimulation, indicating fracture creation. In the gas fracturing without the stimulation, breakdown (complete fracturing) occurs suddenly without any initial leaking, and major fracture planes form along the plane containing principal-stress and intermediate-stress directions, as expected theoretically. However, in the gas fracturing after cryogenic stimulations, breakdown occurred gradually and with massive leaking because of thermal fractures created during stimulation. In addition, the major fracture direction does not necessarily follow the plane containing the principal-stress direction, especially at low confining-stress levels. In tests, we observed that cryogenic stimulation seems to disrupt the internal stress field. The increase in borehole temperature after stimulation affects the permeability of the specimen. When a stimulated specimen is still cold, it maintains high permeability because fractures remain open and local thermal tension is maintained near the borehole. When the rock warms back, fractures close and permeability decreases. In these tests, we have not used proppants. Overall, fractures are clearly generated by low- and high-pressure thermal shocks. The added pressure of the high-pressure thermal shocks helps to further propagate cryogenic fractures generated by thermal shock. Breakdown pressure is significantly lowered by LN stimulation, with observed breakdown-pressure reductions up to approximately 40%.

Introduction

To improve well productivity and hydrocarbon recovery in unconventional plays, almost all horizontal or vertical oil and gas wells are completed with some kind of stimulation. Massive hydraulic fracturing using water-based fluids has been demonstrated as one of the most effective technologies that is widely applied in conjunction with horizontal drilling for developing shale and tight reservoirs (Steward 2013). The commonly used slickwater is prepared by mixing proppants and a minute amount of chemical additives into water, which is readily available and of low cost (Sharma et al. 2004; Shaefer 2005).

Massive hydraulic fracturing using water-based fracturing fluids poses several major challenges. First, water can severely damage the clay-rich shale formations in the sense that clay minerals are apt to absorb water and swell, thus narrowing the conductive fractures and effective pores. Also, capillary retention of water in tiny pores would partially or completely block the flow path of hydrocarbon from the matrix to fracture networks, impairing the relative permeability of hydrocarbons (Mazza 1997; Wang et al. 2016). Second, large quantities of water used in massive fracturing are concerning, placing demands upon local water supply and environments, especially in arid areas with water shortages. Statistics show that during 2009 through June 2011, the median water usage in hydraulic fracturing in Texas for each horizontal well in the Barnett, Eagle Ford, and Haynesville were 10 600, 16 100, and 21 500 m^3, respectively (Nicot and Scanlon 2012). The lower volume of 10 600 m^3 can fill more than two Olympic-size swimming pools or supply water for 65 families for 1 year. Finally, high-pressure injection of fracturing fluids containing chemical additives has caused a contentious community and political climate over groundwater contamination. Different from hydraulic fracturing, cryogenic fracturing using LN offers potentially greater fracturing capabilities without any of these water-related issues.

Cryogenic fracturing is a relatively new technology for unconventional-reservoir stimulation that is meant to expand and supplement the traditional hydraulic-fracturing operations. Cryogenic fracturing exerts a sharp thermal gradient created by contacting a cryogen to a much-warmer rock under reservoir conditions to induce fractures. Cryogen takes a liquid form at low temperatures and transforms into the gaseous phase at standard conditions, such as LN and liquid carbon dioxide (CO_2). Specifically, when LN is injected into a borehole, heat from the rock near the borehole will quickly boil the LN (LN boiling point at atmospheric pressure is −195.8°C or −320.4°F), resulting in rapid cooling and contraction of the near-borehole reservoir rock. Once the contractive tension increases to a sufficiently high level, fractures orthogonal to the rock surface can be started (Cha et al. 2016a). These newly induced fractures can be

This paper (SPE 180071) was accepted for presentation at the SPE Europec featured at the 78th EAGE Conference and Exhibition, Vienna, Austria, 30 May–2 June 2016, and revised for publication. Original manuscript received for review 6 February 2017. Revised manuscript received for review 22 October 2017. Paper peer approved 24 October 2017.

extended farther by high-pressure gas generated from LN vaporization. Note that nitrogen has a liquid/gas expansion ratio of 1:694 at room temperature (20°C or 68°F) and atmospheric pressure.

Although cryogenic fracturing has not been widely deployed during the shale boom, it was tested in a few field pilot tests in the 1980s and 1990s. To improve the recovery of low-permeability sandstone reservoirs, Lillies and King (1982) and King (1983) pumped gelled liquid CO_2 at −28.9 to −40°C (−20 to −40°F) to stimulate wells with standard tubing and casing configurations. The liquid-CO_2 system does not damage formations and reverts to the gaseous state under reservoir temperature. In general, oil and gas wells were cleaned up within 3 to 4 days after the fracturing injections. Because of higher viscosity than pure liquid CO_2, gelled CO_2 was capable of carrying sand proppants to prop open the induced fractures. All the wells that were stimulated with gelled CO_2 showed positive responses in production rates (Lillies and King 1982; King 1983).

In early laboratory studies of LN fracturing, McDaniel et al. (1997) immersed coal samples in LN to observe the cryogenic-fracturing process. The coal samples significantly shrank and broke into smaller cubic fragments as a result of generated or activated microfractures (cleats) orthogonal to the coal surface. It was also found that repeated exposure cycles to LN further broke the coal samples into even-smaller pieces. After three cycles of LN submersion and warmup to ambient temperature, the coal sample tested was reduced to grain-sized particles. McDaniel et al. (1997) then continued fracturing treatment with LN in field tests and reported production rates for five wells before and after the stimulation operations. The results showed that three coalbed-methane wells experienced increased production, one coalbed-methane well showed unchanged production, and one low-permeability sandstone well initially completed with slickwater fracturing decreased in production rate. Grundmann et al. (1998) later treated a Devonian Shale well with LN and observed an incremental production rate of 8% compared with a nearby offset well that was fractured with nitrogen gas. The increased production rate in this field test suggests the efficacy of cryogenic fracturing using LN, but there could be several causes for an offset well in a shale formation to produce at a lower rate, including anisotropic in-situ stresses and heterogeneous formation conditions.

LN and liquid CO_2 have low viscosities (Rudenko and Schubnikow 1968; Fenghour et al. 1998), and therefore they cannot carry conventional high-density proppants normally carried by viscous fluids. Gupta and Bobier (1998) suggested that it is possible to increase the injection rate of liquid CO_2 to improve proppant-transport efficiency, although normally it is incapable of transporting adequate proppant. The turbulence caused by high flow rate allows sufficient suspension of common proppant, at least from the wellbore into the perforation clusters, if not through the outreaching fractures (Gupta and Bobier 1998). Some studies even showed that cryogenic fracturing might rely less on proppant compared with conventional hydraulic fracturing. The experiments of McDaniel et al. (1997) demonstrated that coal rubblization after cryogen contact could act as a self-propping mechanism. That is, if the fracture-plane rock experiences sufficient thermal-induced breakage, then the rubblized particles may prop the fracture open against in-situ stresses during the warmup and closure of the cryogenic fractures. Even if neither conventional proppants nor self-propping mechanisms can effectively take place, ultralightweight proppants (ULWPs) may be a good candidate to be tested. ULWPs are chemically synthesized proppants consisting of a hardened core with multiple layers of outer resin coating (Kendrick et al. 2005). With ULWPs, Kendrick et al. (2005) obtained improved post-treatment production rates from wells stimulated by nitrogen foam in Devonian Shale. Compared with those treated with traditional proppants, the majority of the wells treated with ULWPs performed as well or even better.

During the past 2 decades, no further studies have been conducted to better understand and apply cryogenic-fracturing technology. The fracturing mechanisms and major factors controlling cryogenic-fracturing processes are poorly understood. With the increasing development of unconventional reservoirs and the rising cost of acquiring water in some plays, it is necessary to conduct research to further investigate this water-free, and hence formation-damage-free, and environment-friendly fracturing technology and to discover the significant potential it can provide for the oil and gas industry. This study aims to better understand and optimize the cryogenic-fracturing processes using LN and discusses how it can be integrated into our current fracturing technology to enhance the oil and gas recovery from unconventional oil and gas reservoirs.

Simple preliminary cryogenic tests were conducted to understand the LN and material behaviors by performing submersion tests and applying LN to boreholes in unconfined concrete specimens (Cha et al. 2014). Data gathered from the previous study provided a basic understanding of physical mechanisms. In this study, we investigated the effect of cryogenic stimulation on rock fracturing under true triaxial-confining stresses. We developed laboratory setups and procedures that are designed for conducting cryogenic-fracturing tests under wellbore conditions. In these tests, LN was flowed through boreholes drilled in rock blocks including concrete, shale, and sandstone under triaxial-confining stresses. Fracturing processes were thoroughly monitored to observe the behaviors associated with cryogenic treatment. Fracture development was assessed by acoustic measurements, permeability measurements, and visual inspection. Comparisons were made between conditions before and after stimulation to evaluate the efficiency of this technique. The results will help to select efficient applications of cryogenic stimulations as a stimulation technique and will set the foundations for continuing avenues of research.

Laboratory Studies

The devices and procedures used in our tests are significantly optimized and improved as a result of understanding cryogen and fluid behavior from our preliminary studies. Artificial and natural rock specimens were prepared for the experiments. Shale and sandstones were obtained from outcrops of oil- and gas-producing formations.

Experimental Equipment. A laboratory system for cryogenic-stimulation study under true triaxial-loading conditions has been developed. It consists mainly of a triaxial-loading device, an LN delivery, and control/measurement system **(Figs. 1 and 2).** More details of the laboratory system are reported in Cha et al. (2017).

Triaxial-Loading System. The true triaxial-loading system was developed to simulate the effects of stress levels and anisotropies manifested in situ on the characteristics of cryogenic fracturing. The containment was designed for the selected specimen size 8×8×8-in. The true triaxial-loading system can load the specimen up to 4,500 psi along the *x*-axis and *y*-axis, and 6,000 psi along the *z*-axis, and we can independently control loadings on the three axes. Three pneumatic pumps power the two hydraulic actuators (*x*-axis and *y*-axis) and the hydraulic press (*z*-axis). One advantage of the system is the vertical load frame can be moved by rolling sideways on the bed. This provides space to work on specimens inside the containment. An open system (outer surface of the specimen under stress, but not under fluid pressure) is preferred in our study to better manage unexpected conditions such as a cryogen spill, and for application of instrumentation (Fig. 1).

Polytetrafluoroethylene (PTFE) or silicon pads were placed between specimens and the loading platens to provide as uniform contact and loading as possible to specimen surfaces. PTFE or silicon pads resist temperature down to −350 and −80°F, respectively. A servo-control system for automatic load control is not available on our device and is not required because the loadings are quasistatic.

Constant forces were achieved by manual control or in a quasiautomatic manner using pressure-relief valves attached to the hydraulic lines. In the manual-control tests, when a certain amount of pressure decay occurs in the hydraulic system, a small amount of pressure is added by pumping accordingly.

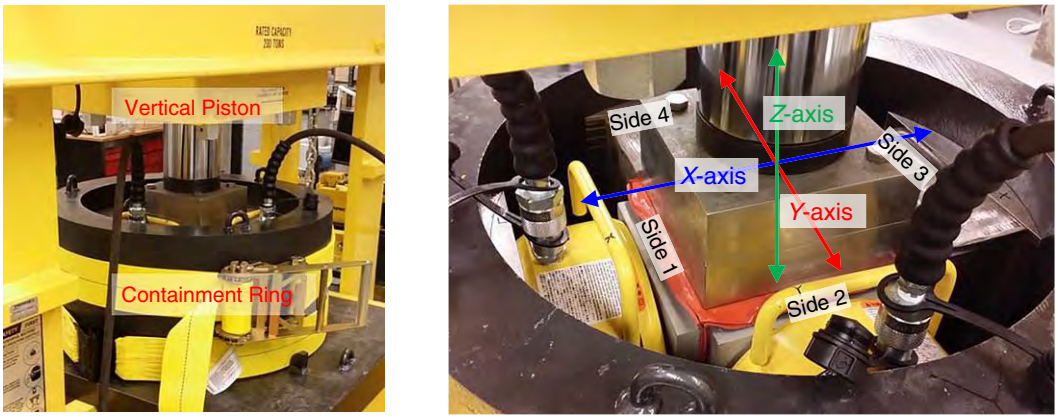

(a) (b)

Fig. 1—True triaxial-loading device: (a) containment ring housing the specimen and actuators; (b) close-up inside the ring showing the axes and the faces of the specimen.

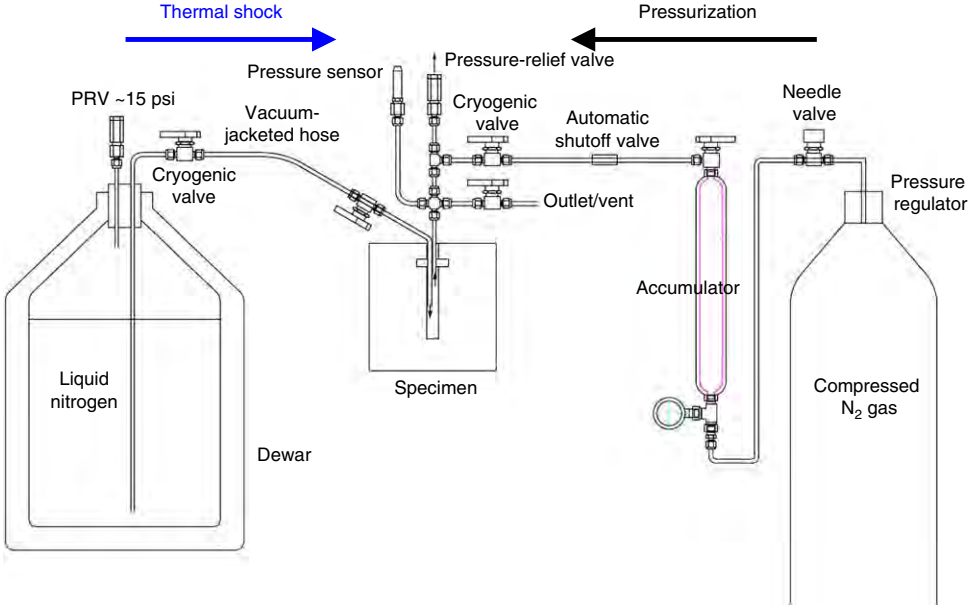

Fig. 2—Cryogenic-fracturing schematic (true triaxial-loading system not shown).

LN Delivery. The cryogen flows from the dewar once an outlet valve is opened by the nitrogen-gas pressure generated inside the dewar (Fig. 2). This pressure was usually maintained at low levels of approximately 10 to 20 psi. The fluid-injection/delivery system for cryogenic stimulations needs to be fundamentally different from that for hydraulic fracturing. For cryogenic thermal fracturing, cryogen needs to flow through and be replenished to decrease the temperature of boreholes because LN will rapidly vaporize, obtaining its heat of vaporization from the much-hotter rock. Compressed nitrogen gas was used to push LN into boreholes under higher pressure (termed here as "higher-pressure LN flow") and pressurize boreholes to perform the breakdown test. Pressure can be applied as shown on the right-hand side of Fig. 2.

Tubing and fittings in the cryogen-transport lines must withstand cryogenic temperature (down to −321°F in our study). We used stainless-steel 316 and brass for cryogen transport, which provide such an ability because their brittleness/ductility-transition temperature is lower than the LN boiling point. Stainless steel has a higher pressure rating at the cryogenic temperature than brass. Tubing for higher-pressure applications at the cryogenic temperature must be seamless and annealed. 1-in. stainless-steel tubing was used for borehole casing in our tests and is affixed to the borehole wall by epoxy for sealing and pressure resilience. Epoxy generally worked well for that purpose but could deteriorate after three to five cycles of LN exposure. Insulation was applied to the lines between the dewar and specimen inlet to minimize heat transfer.

Measurements and Monitoring. Measured parameters include pressure, temperature, LN consumption, and photos of specimen surfaces. The pressure was recorded through a pressure sensor placed at the end of a standoff tube (Fig. 2), where a vapor cushion hinders conductance of the cold temperature to the sensor. Data show that the temperature at the tip of the standoff tube is greater than 0°C throughout the stimulation **(Fig. 3).** The tube is not to be longer than necessary because a long narrow tube creates drag and thus decrease responsiveness to rapidly changing pressure. For temperature measurement, T-type thermocouples were chosen for accuracy and range. Very thin thermocouple wires were inserted into the borehole between casing and borehole walls. One thermocouple hangs in the borehole to measure temperature in the borehole, and another is attached to the borehole wall to observe the temperature of the wall. LN consumption was measured by putting the dewar on a balance. In addition, acoustic waves were used for assessments of fractures before and after treatments.

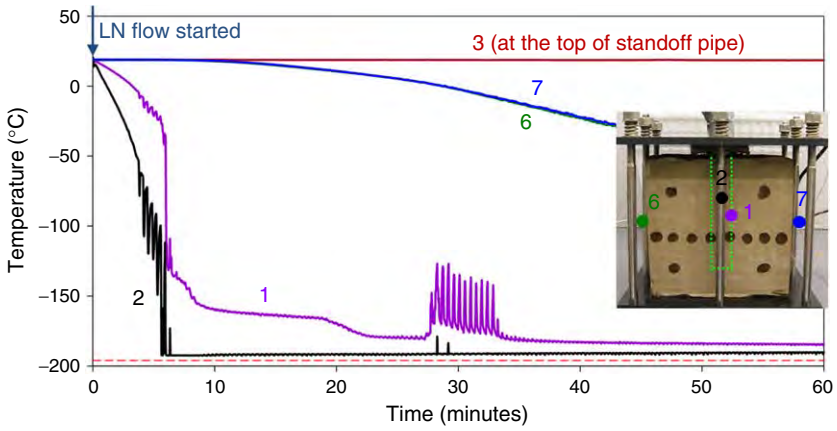

Fig. 3—Temperature data from five thermocouples during a low-pressure LN borehole flow-through for an unconfined specimen. Locations of thermocouples are shown in the inset.

Test Procedures. Cryogenic stimulations are accomplished by applying LN to the borehole in a specimen. Baseline conditions of a specimen relevant to fracture indications were measured before treatments, and then the same measurements were performed during treatments or after completing the treatments to allow comparisons. Assessments of fractures include acoustic waves, pressure decay, and visual observations.

Stimulation Procedures. As stated previously, boiling LN is needed to lower temperature and the cryogen needs to be continuously flowed through the borehole. Using the cryogenic-fracturing apparatus under true triaxial loading, we performed two cryogenic-stimulation schemes: low-pressure LN flow and high-pressure LN flow. In the scheme of low-pressure LN flow, LN was flowed from the dewar because of a pressure difference between the inside and the outside of the dewar upon opening the dewar outlet valve. Pressure ranged from 5 to 20 psi in the borehole, depending on the internal pressure of the dewar. In the high-pressure scheme, LN was flowed through the borehole under higher pressure (300 to 400 psi) for quicker cooling in the borehole because of increased gas density and reduced film-boiling effects. In the scheme of high-pressure flow, the higher borehole pressure may facilitate the fracture opening by helping to reach tensile strengths of specimens. Typically, higher-pressure stimulations were applied multiple times because our vessel for storing LN for higher-pressure injection is small (1 L), which makes each stimulation cycle very brief (1 to 2 minutes). Nitrogen, which was liquid before entering the borehole, initially exits the borehole as gas and later as a gas/liquid mixture as the borehole cools. Gas/liquid leaving the borehole was not recovered in either stimulation scheme.

Assessments of Fractures. Assessments of fractures were made by borehole-pressure-decay tests, acoustic measurements, and breakdown pressures (P_{BD}). Borehole-pressure-decay tests were performed by applying pressure to the borehole, shutting the borehole in, and monitoring the pressure decay. This was done before cryogenic treatments, between treatments, and after completing the cryogenic treatments. After all planned stimulations were completed for a specimen, the specimen was subject to a high gaseous-nitrogen (GN) pressure to fully fracture ("breakdown") the block. The P_{BD} values of different treating schemes were compared with the baseline P_{BD} of the non-LN-treated specimen. Breakdown tests were performed last because they fully fracture the specimens.

Transmission of compressional (*P*-waves) and shear (*S*-waves) acoustic waves were recorded before and after the treatments. Post-stimulation measurements were performed before applying the final P_{BD}, so that we can quantify the effect of cryogenic stimulations. The characteristics of acoustic waves propagating through the medium depend on the mechanical properties of the medium. In particular, the wave velocity in jointed rock masses is a function of the density of fractures (or fracture spacing) (Cha et al. 2009). When other properties such as intact rock properties, density, and joint stiffness are the same, the wave velocity can be used as a monitoring tool to characterize fracture generation.

Specimens. ***Collection and Preparation.*** Shale and sandstone were collected from outcrops of oil- and gas-producing formations to make specimen types more relevant to the purpose of this study. Specifically, we used Niobrara shale blocks gathered from an outcrop of the Niobrara Formation in Lyons, Colorado, and sandstone blocks gathered from an outcrop of Williams Fork Formation in Western Colorado. A fairly large specimen size (8×8×8 in.) was selected for the study so that sufficient thermal gradients could be created inside the specimen for an extended time, which may be required for thermal tensile fracturing. They were precisely cut into the desired size using a bridge saw (Cha et al. 2016b).

Concrete specimens made of cement and sand were used as surrogates for rocks. A fresh concrete with a water/cement ratio of 0.55 and sand/cement ratio of 2.5 was mixed and poured into an 8-in. cubic mold and sealed in a plastic bag. After 24 hours, the seal and mold were removed, and the concrete block was cured under water (*ASTM C192/C192M-16a* 2014a) for at least 2 months, which maximizes hydration-enhancing concrete strength.

Before cryogen stimulations, a 1-in.-diameter borehole was drilled into prepared 8×8×8-in. specimens using a diamond coring drill bit with 1.06-in. diameter under dry conditions, and the borehole was drilled to a depth of 6 in. A 1-in. stainless-steel 316 casing was then attached to the borehole with epoxy after the thermocouples were inserted into the borehole. The casing extends 2 in. into the borehole.

Intact-Rock Properties. Basic index properties of intact specimens are listed in **Table 1.** Key intact-rock properties were obtained and may allow more-quantitative approaches to further analyze results. Mechanical, thermal, and flow properties of the specimens were tested and obtained. Porosity and permeability were measured using a CMS 300 automated permeameter (CoreLab, Houston). Dynamic elastic constants were calculated from densities and acoustic-wave velocities (Cha and Cho 2007). Static Young's modulus, unconfined uniaxial-compressive strength, and splitting tensile strength were measured according to the ASTM standards (*ASTM D3967-16* 2008; *ASTM D7012-14e1* 2014b). Specific heat capacities were measured using a calorimeter, and linear thermal-expansion coefficients were measured using core specimens.

	Rock Type		
Properties	Concrete	Sandstone	Shale
Density (g/cm^3)	2.04	2.18	2.39
Unconfined compressive strength (psi)	5.41×10^3	6.02×10^3	7.92×10^3
Splitting tensile strength (psi)	0.42×10^3	0.65×10^3	1.23×10^3
Static Young's modulus (psi)	3.8×10^6	–	6.0×10^6
Dynamic Young's modulus (psi)	4.4×10^6	6.5×10^6	6.9×10^6
Dynamic shear modulus (psi)	1.8×10^6	2.7×10^6	2.7×10^6
Poisson's ratio	0.24	0.22	0.27
P-wave velocity (m/s)	4220	4850	4970
S-wave velocity (m/s)	2455	2906	2796
Specific heat capacity [J/(kg·K)]	891	857	990
Linear thermal expansion coefficient (K^{-1})	1.3×10^{-5}	–	1.1×10^{-5}
Porosity (%)	9.56	11.5	6.64
Permeability (md)	8.72×10^{-3}	0.349	1.06×10^{-3}

Table 1—Mechanical, thermal, and flow properties used for cryogenic-fracturing test under confinement.

Results and Analyses

Eight concrete specimens, four shale specimens, and two sandstone specimens were tested under different triaxial-confining stresses and with different cryogen-treatment procedures, as shown in **Table 2.** The results are analyzed, compared, and discussed here. In what follows, we will first present measurements of temperature and pressure in boreholes during treatments and subsequent breakdown tests, and then present the effects of cryogenic stimulations on fracture patterns, permeability changes, and acoustic data.

Temperature and Pressure in Boreholes. Breakdown tests were first performed on untreated specimens, Nos. 16 and 17. In these tests, GN was used to pressurize the borehole and fracture the specimens **(Fig. 4).** The breakdown pressures (P_{BD} values) were recorded as the baseline P_{BD} to be compared with those for specimens stimulated with LN. Breakdown by gas pressure on untreated specimens is characterized by a sudden loud fracture without any preleaking of gas. Indications of specimen fracture were also noted from the pressure response in the hydraulic lines connected to the loading actuators. As exemplified in Fig. 4b, the *x*-axis hydraulic line responded to the breakdown with a high jump in the hydraulic pressure. This brief jump in the *x*-direction is caused by the sudden opening of the fracture in the minimum horizontal-stress direction (*x*-axis) (fractures propagated along a plane perpendicular to the minimum horizontal-stress direction), as confirmed later by visual inspection of the fractures. Fracture creation and propagation was so sudden that the loader did not have enough time to maintain constant load.

Figs. 5 and 6 present typical temperature and pressure evolutions during low-pressure LN flow and high-pressure LN flow through boreholes. For low-pressure injection, the temperature dropped quickly; however, on the borehole wall, the rate of temperature drop is retarded compared with that of the borehole (Fig. 5a) because of the Leidenfrost effects (film boiling). Cryogen pressure in the borehole remained low (10 to 15 psi) (Fig. 5b). For high-pressure injection, the temperature dropped more quickly than for the low-pressure treatment because of the reduced effect of surface film boiling under higher-pressure flow-through (Fig. 6a; red curve initially overlies blue curve). The cryogen pressure during the flow-through was 250 to 450 psi, but very briefly, approximately 1 to 2 min (Fig. 6b). For high-pressure treatment, multiple cycles of LN treatment were performed because of the small volume of the LN container (1 L) and thus the small amount of LN available for each treatment. Upon ceasing the LN supply, the temperature in the borehole increased quickly back after these durations of stimulations.

Although probably a test artifact, the temperature reduction in the borehole wall was slower in the unconfined-specimen tests than the confined-specimen tests (compare Fig. 3 with Fig. 5). This could be because of the contraction of borehole-wall circumference when subjected to high confining stresses; the thermocouple, which was attached to the wall before the application of stresses, may have been loosened and the quality of adhesion may have been compromised by the contraction, and thereby the thermocouple experienced more-rapid cooling.

In GN fracturing of untreated specimens, no preleaking of gas was noticed before breakdown. For cryogenically treated specimens, however, before reaching the breakdown points, very noticeable high-pitch hissing sounds that increased with increasing borehole pressurization were heard, indicating leakage and potentially also the progression of fractures.

We performed tests that showed cryogen leaking during cryogenic stimulation, which means local breakthrough by cryogenic stimulation only. This occurred in both low- and high-pressure injections; the approximate times for major leaking to appear are indicated by the dotted arrows in Figs. 5b and 6b. In higher-pressure LN flow, leaking of LN was noted during the third high-pressure LN stimulation, indicating that fractures created were significant and they have extended to the surface at least locally.

Specimen No.	Specimen Type	Stresses (x:y:z) (psi)	Test Procedure	Measured P_{BD} (psi)	Notes
16	Concrete	500:750:1,000	Fracturing by GN	583*	* Weakness created near the casing
17	Concrete	500:750:1,000	Fracturing by GN	1,180	–
18	Concrete	500:750:1,000	Low-pressure LN flow (30 minutes) + fracturing by GN	685	–
19	Concrete	500:750:1,000	High-pressure LN flow + fracturing by GN	778	–
20	Concrete	500:750:1,000	High-pressure LN flow + fracturing by GN	759	–
21	Concrete	1,000:1,500:2,000	Fracturing by GN	1,317	–
22	Concrete	1,000:1,500:2,000	Low-pressure LN flow (30 minutes) + fracturing by GN	–	–
23	Concrete	1,000:1,500:2,000	High-pressure LN flow + fracturing by GN	1,094	–
S1 (24)	Shale 1	1,000:1,500:2,000	Low-pressure LN flow (40 minutes)		CT scanned before and after the LN test.
			High-pressure LN flow	1,394	Three LN treatment cycles.
S2 (25)	Shale 2	1,000:3,000:4,000	High-pressure LN flow (first round)	1,417	Three LN treatment cycles for each round. LN flowed until getting similar decay curves at last runs.
			High-pressure LN flow (second round)		
S3 (26)	Shale 3	1,000:1,500:2,000	Low-pressure LN flow (40 minutes)	–	Pressure decay before and after show a permeability enhancement.
			High-pressure LN flow	168	Fractured at early stage when doing pressure decay before testing and before loading (fractured at 180 psi)
S4 (27)	Shale 4	1,000:1,500:2,000	Fracturing by GN	2,439	–
SS1	Sandstone	1,000:1,500:2,000	High-pressure LN flow	219	Fractured during pressure-decay test when σ_z = 60 psi.
SS2	Sandstone	σ_z = 60 psi	Fracturing by GN	689	–

Table 2—Matrix of cryogenic-fracturing experiments performed under triaxial-confining stresses.

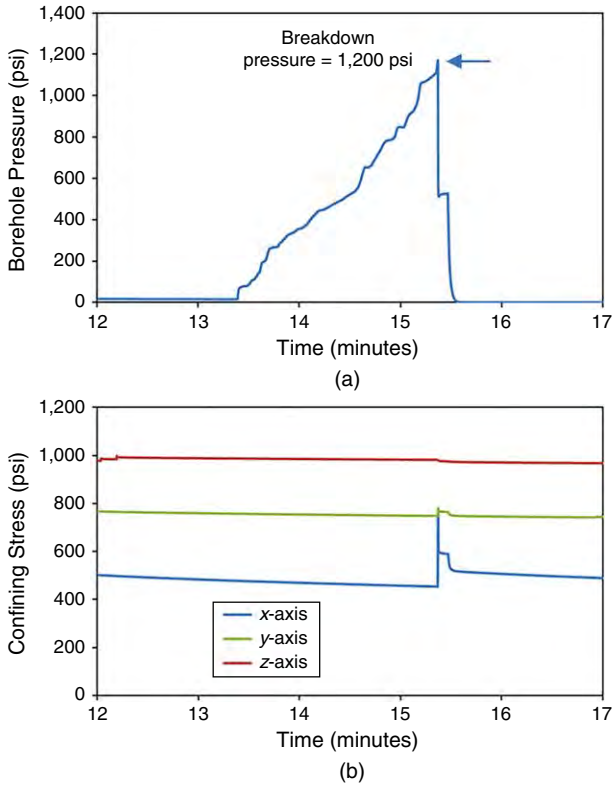

Fig. 4—Breakdown-fracturing test (using gas pressure) of a specimen without LN treatment (Specimen No. 17).

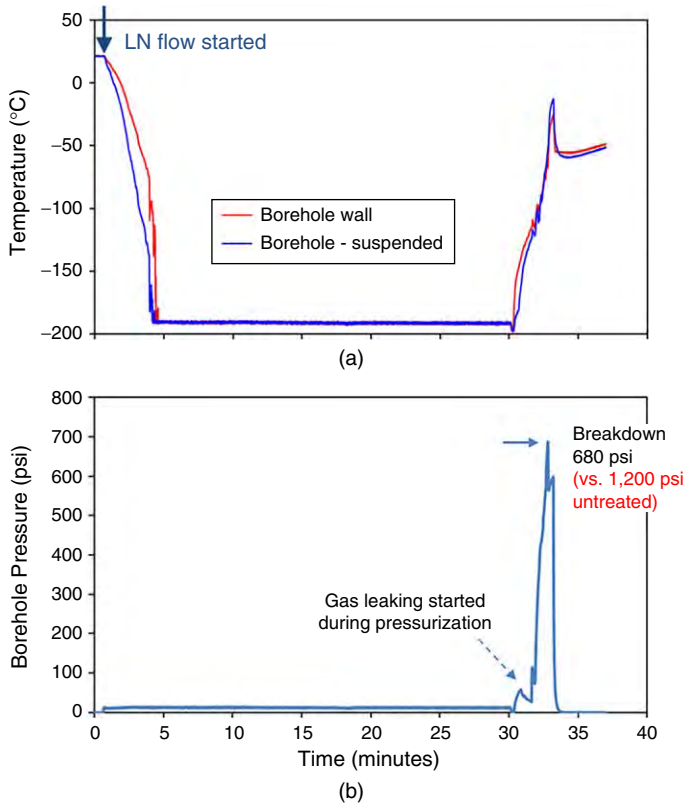

Fig. 5—Temperature and pressure during low-pressure LN flow-through (Specimen No. 18).

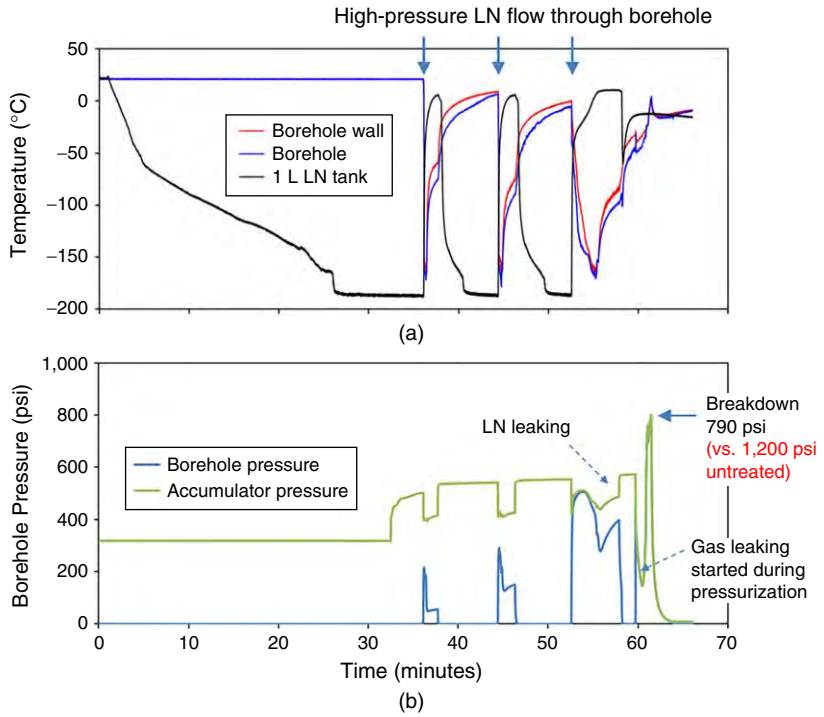

Fig. 6—Temperature and pressure during higher-pressure LN flow-through (Specimen No. 19).

Fig. 7 summarizes and compares breakdown pressures (P_{BD}) of tested shale and concrete specimens. This clearly indicates that cryogenic treatment decreases the magnitude of P_{BD} in concrete and shale specimens by both low- and high-pressure LN flow-through. P_{BD} reductions observed are 37% for the concrete specimens and 43% for the shale specimens. Bedding/existing cracks can lead to significantly lower P_{BD} with or without treatment.

In the breakdown tests, the gas pressure was applied to the borehole until breakdown. Because of the use of gas and the volume in the tubing and borehole, injection-system compliance is sizable (Lecampion et al. 2016). In the case of untreated specimens, the energy stored in the compressed gas may make the pressure level of fracture start similar to the breakdown pressure, and breakdown immediately follows the fracture creation (Detournay and Carbonell 1997; Lhomme et al. 2005). Indeed, we observed a sudden and loud sound

for all untreated specimens with a sudden drop in borehole pressure. In cryogenically treated specimens, thermally induced fractures already exist near the borehole. Upon applying pressure to approach the breakdown, we observed audible gas leakage that increases with increasing pressure. When pressure reached the level needed to propagate the thermally induced fractures, breakdown took place. These breakdown pressures for the treated specimens are lower than those of the untreated specimens.

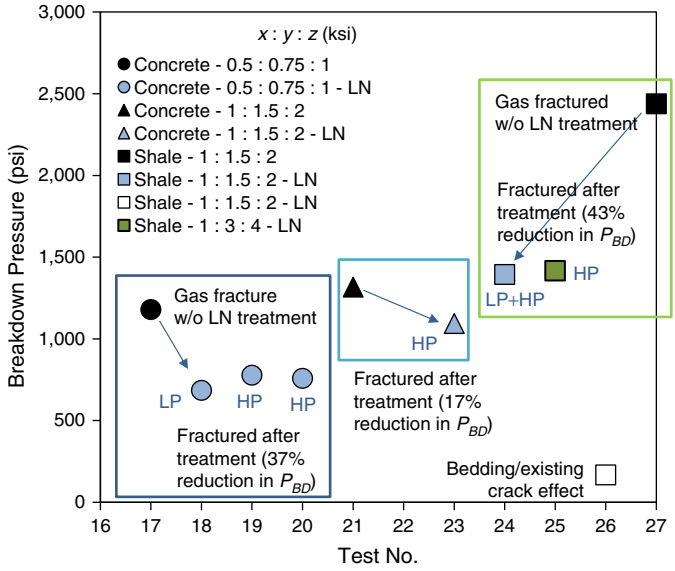

Fig. 7—Effect of cryogenic stimulation on breakdown-pressure levels for different rocks and stimulation conditions. LP and HP denote low- and high-pressure LN flow. See Table 2 for details.

Fracture Patterns. Cryogenic stimulations alone generally did not lead to fracture propagation to the surface of the specimens; it was only in some long-duration stimulations that fractures propagated to the external surface. These were identified visually and/or by localized leakage of nitrogen during stimulation. Most fractures reached the surface because of the breakdown of the specimens. In this subsection, we present fracture patterns visible on the external surfaces of specimens after breakdown.

Untreated Specimen: Direction of Breakdown Fractures. Breakdown fracturing of untreated specimens tended to be sudden, without any preleaking. The major fracture direction in the untreated specimens was perpendicular to the minimum horizontal-stresses direction (i.e., x-axis) from the borehole wall **(Fig. 8).** In other words, major fracture planes tended to exist along the y–z plane, which is the plane containing the maximum-principal-stress direction and the intermediate-stress direction. This behavior is expected from rock mechanics and is also observed in hydraulic fracturing. The top-view picture taken from inside the wellbore after breakdown also shows the fractures propagating perpendicular to the minimum horizontal-stresses direction from the borehole wall (the upper subset photo in Fig. 8a).

Effect of Cryogenic Stimulations on Direction of Fractures. We observed that if specimens are cryogenically stimulated, the breakdown-fracture direction could deviate from the conventionally predicted directions. This is particularly true when the confining stress is low. For example, fractures were in rather arbitrary directions **(Figs. 9a and 9b),** or occurred only locally (Figs. 9c and 9d). The triaxial-stress ratios of these blocks were $x{:}y{:}z = 500$, 750, and 1,000 psi for Figs. 9a and 9b and $x{:}y{:}z = 1{,}000$, 1,500, and 2,000 psi for Figs. 9c and 9d. In Fig. 9b, the fracture opened in a half-wing configuration along the minimum horizontal-stress direction. Another fracture wing was along the maximum horizontal-stress direction. In Fig. 9d, the main fracture propagation was around the wellbore, affected by the casing's much-higher thermal conductivity, creating weakness in that region. These fractures occurred gradually without clear fracturing sounds and with massive preleaking. Clearly, cryogenic stimulation disrupts the internal stress field.

However, with larger stress anisotropy (and perhaps larger stress magnitude relative to a thermal treatment applied) in triaxial-confining stresses, fractures did follow theoretically predicted directions; the fractures propagated as expected, in a plane perpendicular to the minimum horizontal stress (x-direction). At even-larger stress anisotropy, we surmise that confining stress would again govern the fracture direction (**Fig. 10;** triaxial stress $x{:}y{:}z = 1{,}000$, 3,000, and 4,000 psi). A comparable behavior in hydraulic fracturing in a medium with natural fractures may be that when the horizontal-stress difference increases, the fracture is smoother and straighter (Beugelsdijk et al. 2000; Guo et al. 2014).

Deviation from the directions expected from stress principles may lead to more fracture tortuosity or complexity than pressure-based fracturing as observed in Figs. 9 and 10, and also in Cha et al. (2016a). This tortuosity or complexity may affect the fluid flow path, self-propping, and the efficiency of stimulations. On the other hand, as shown in Cha et al. (2016a), fully developed thermal fractures in a wellbore extend both longitudinally and radially away from the wellbore, and with tortuosity tendency, they form a rather complex network.

Cryogenic Fractures as "Seed Fractures" for Pressure-Induced Fracturing. After the breakdown tests, specimens were separated along the major fractures, and fracture surfaces were visually inspected. There were clear discontinuities that indicate that part of the fracture surfaces was cryogenically induced and part of the fracture surfaces was opened up by the high P_{BD}. The surfaces of the cryogenically opened fractures are adjacent to the borehole and are slightly rounded, while the surfaces opened up by high gas pressure are straighter (Fig. 10). This sequence suggests that cryogenic stimulation created "seed" fractures that did not fully extend to the external surface (except the top portion). These seed fractures, however, significantly lowered the P_{BD}, as presented previously. The creation of seed fractures was likely responsible for the preleaking observed during applications of breakdown pressures to the boreholes. It should be noted that many sets of seed fractures may have been generated. Only a major one, however, was activated by the breakdown pressure and eventually led to the separation of the specimen. Having multiple seed fractures starting from and adjacent to the borehole is favorable from the production's point of view because they improve the permeability near the borehole and not just along the primary fracture. When the specimen was not treated with LN, only a sharp straight fracture formed from the borehole to the block surfaces; no discontinuities in the surface morphology were observed **(Fig. 11).**

Permeability Changes. After each treatment procedure, enhancements in the permeability were assessed by borehole-pressure-decay tests. During the application of confining stress on both our concrete and shale, permeability decreased with stress increment (Alqatahni et al. 2016).

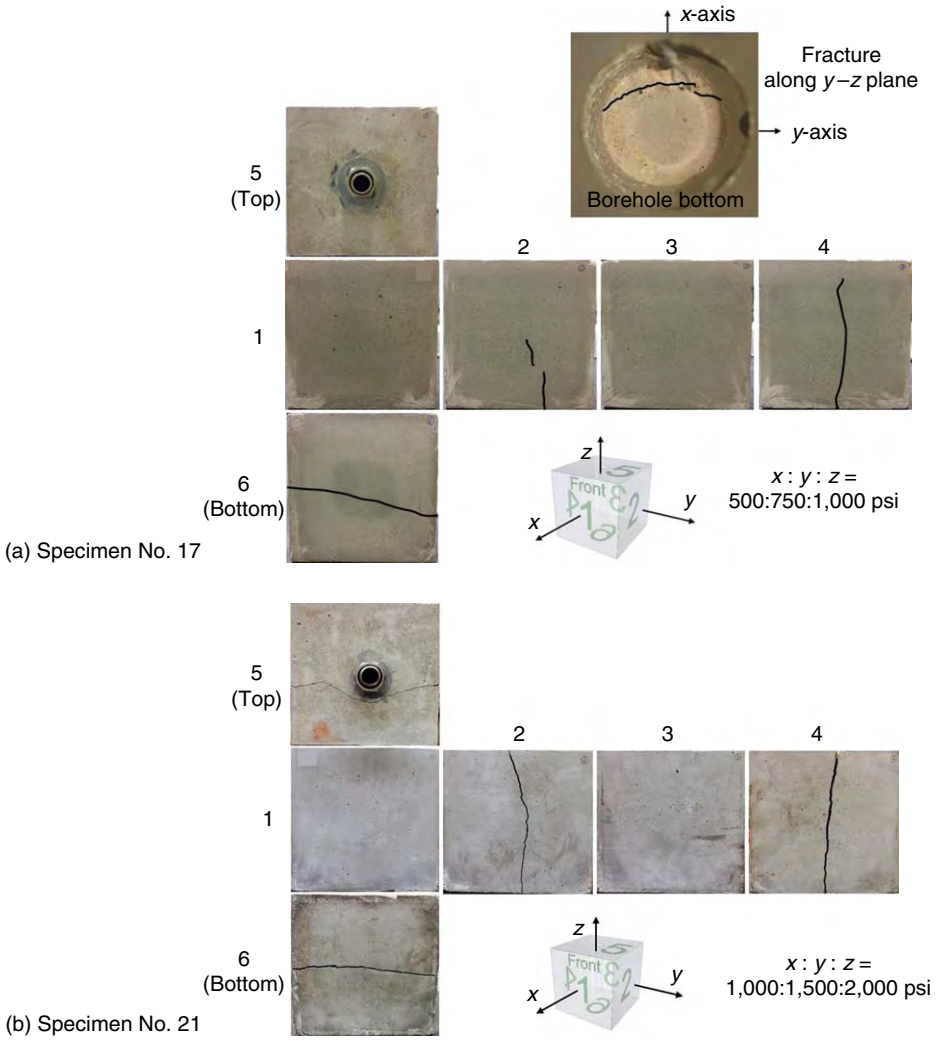

Fig. 8—Block surfaces after breakdown fracturing (using GN) without LN stimulation. Note that fractures are along the *y–z* plane (i.e., the plane with the principal-stress and intermediate-stress directions). Breakdown fractures occurred suddenly without any preleaking. (a) Specimen No. 17; (b) Specimen No. 21.

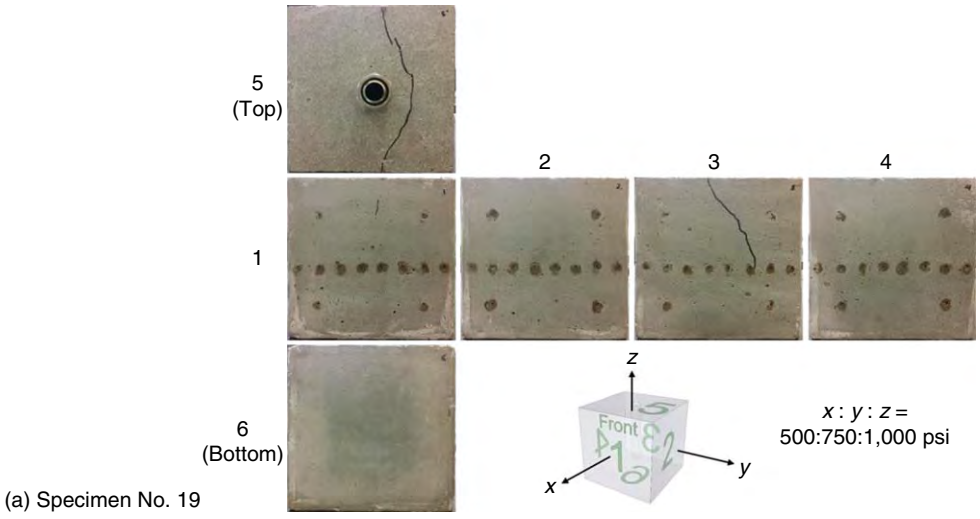

Fig. 9—Block surfaces after breakdown after LN stimulations. Fractures do not follow *y–z* plane, and are in rather arbitrary directions (a, b), or occurred only locally (c, d). The breakdown occurred more gradually with significant preleaking. (a) Specimen No. 19; (b) Specimen No. 20; (c) Specimen No. 22; and (d) Specimen No. 23.

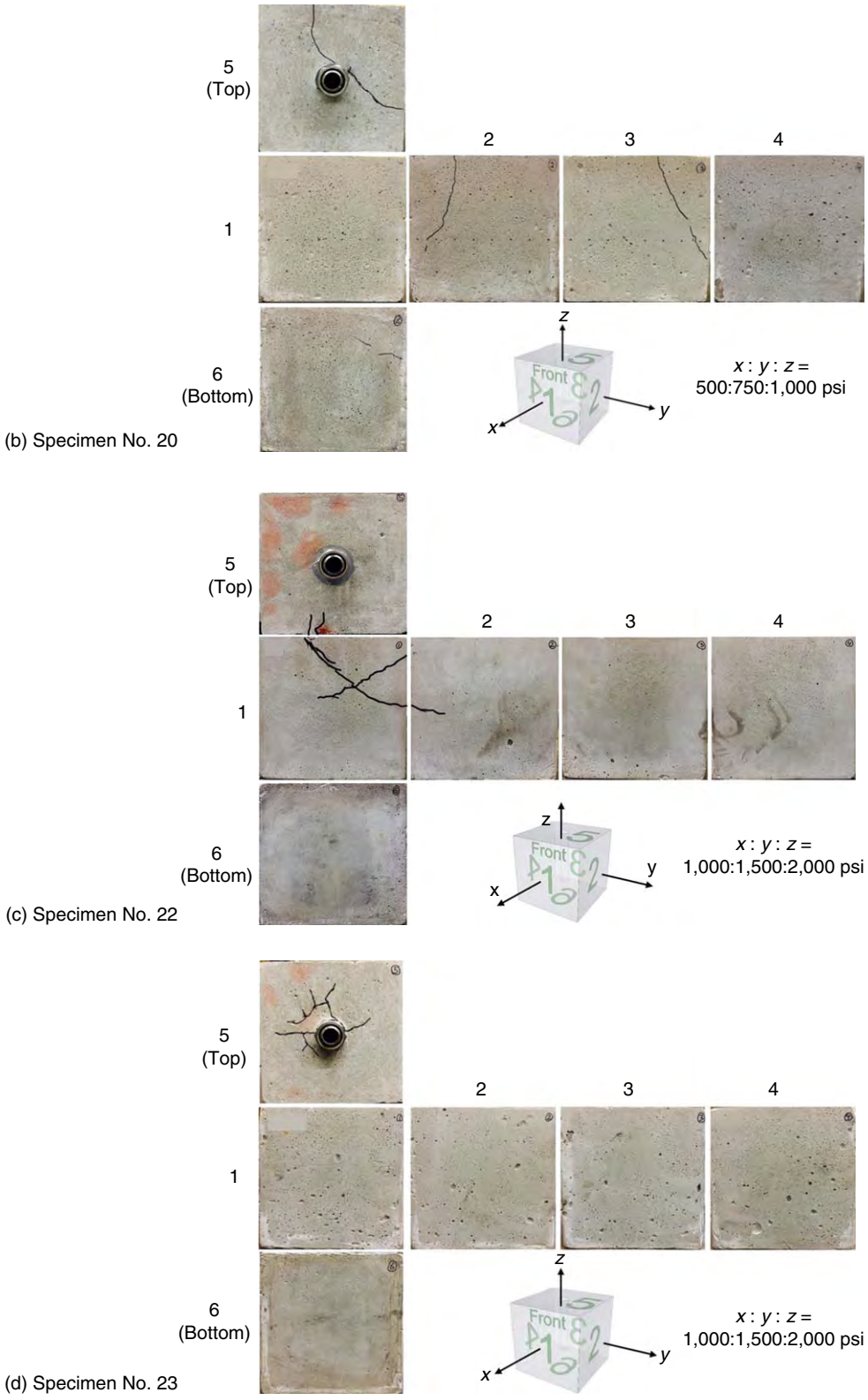

Fig. 9 (continued)—Block surfaces after breakdown after LN stimulations. Fractures do not follow *y–z* plane, and are in rather arbitrary directions (a, b), or occurred only locally (c, d). The breakdown occurred more gradually with significant preleaking. (a) Specimen No. 19; (b) Specimen No. 20; (c) Specimen No. 22; and (d) Specimen No. 23.

Permeability Increase Caused by Cryogenic Treatment. Permeation (pressure decay) profiles clearly show that low- and high-pressure LN flow increased the permeability of treated specimens. In one test, LN flowed under low pressure for 36 minutes resulted in a significant permeability increase (**Fig. 12a),** indicated by a more-rapid pressure decay. Three cycles of higher-pressure LN flows under triaxial loading also led to significant permeability enhancements. We observed that repeated cryogenic stimulations increased permeability further, indicating that each LN-treatment cycle created new fractures and/or widened existing fractures. Fig. 12b is an example of a higher-pressure LN flow test, where greater permeability was achieved after each brief LN cycle.

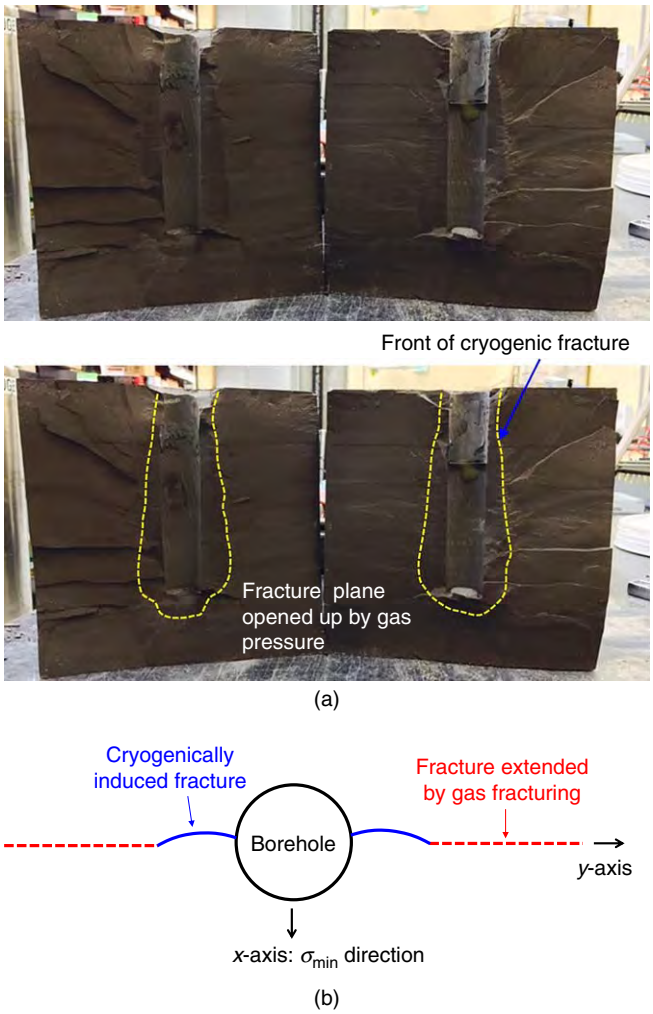

Fig. 10—Fracture plane after breakdown fracturing of LN-treated shale specimen (Specimen No. S2). (a) Yellow dotted lines show the front of cryogenically created fractures. (b) Depiction of fractures at the midheight of the shale block: slightly curved nature of cryogenically induced fractures and straight fractures extended by gas fracturing.

Fig. 11—Fracture plane after breakdown fracturing of the untreated-shale specimen (Specimen No. S4).

Effect of Temperature. We also observed the effect of temperature on the permeability of the specimen that experienced cryogenic stimulation. Permeability decreased when the specimen returned to the room temperature after the low-pressure treatment (Fig. 12a) and after the third high-pressure LN flow (Fig. 12c). When the temperature of the specimen was low, the specimen was in the state of local thermal contraction near the borehole, and fractures should remain open around the borehole. As the specimen warmed, the thermally induced stresses relaxed and fractures closed, reducing the permeability of the specimen.

In contrast, in untreated specimens or weakly treated specimens, the permeability was lower when the specimen was at a lower temperature and increased when it returned to the room temperature. In other words, if no fracture exists near the borehole, permeability is lower at a lower temperature. At low temperature, the specimen is under thermal contraction, and consequently, the pore sizes are reduced, and perhaps the natural fracture widths are also smaller. This behavior was sometimes observed after the first cycle of brief high-pressure flow-through.

Acoustic-Wave Signature. Changes in the specimens' ability to transmit acoustic waves before and after stimulations were examined. Acoustic waves were measured between Faces 1 and 3 and Faces 2 and 4, which are pairs of opposing faces **(Fig. 13a).** Fig. 13b shows

the 12 locations of the acoustic actuators and receivers on a specimen surface. We observed that acoustic velocities and amplitudes decrease (original amplitudes not shown) after cryogenic treatments, indicating fracture creation in the specimens. For shale specimens, we also observed the effect of layering on the velocities and attenuations.

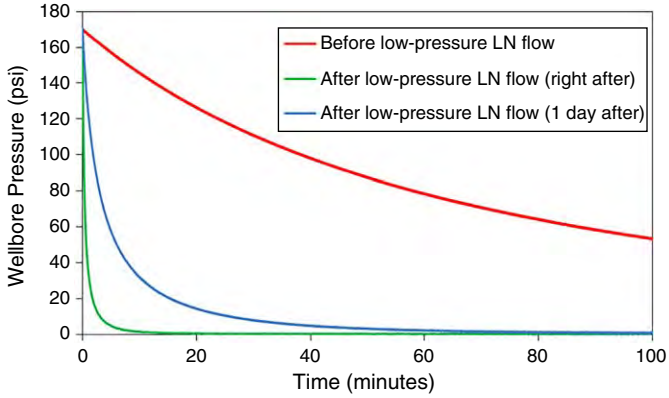

(a) Effect of low-pressure LN flow on permeability (specimen unconfined except 60-psi vertical loading). More rapid pressure loss indicates higher permeability.

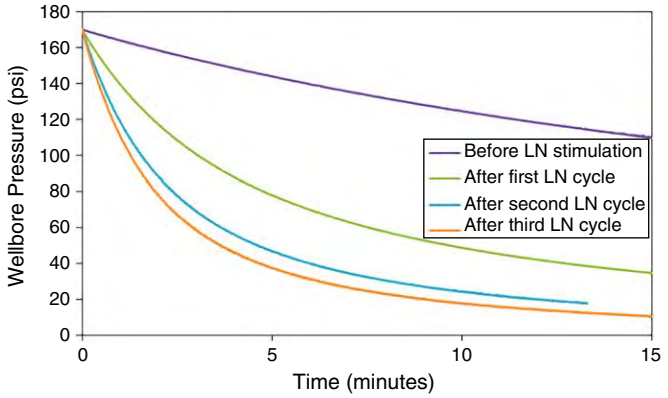

(b) Effect of repeated high-pressure LN flow on permeability (under confining stresses).

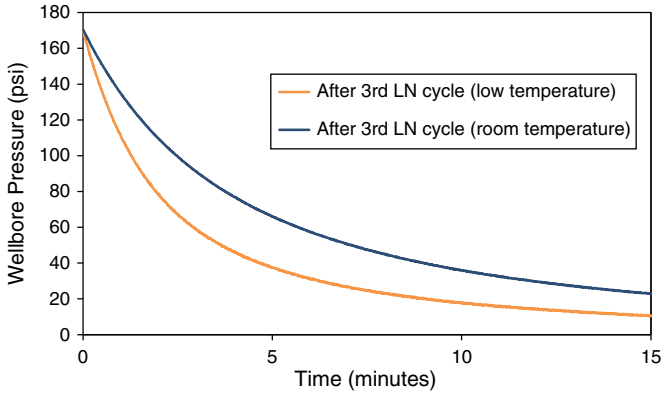

(c) Effect of specimen temperature on permeability (under confining stresses).

Fig. 12—Effect of cryogenic treatment on permeability changes (Specimen No. S1, Table 2). (a) Effect of low-pressure LN flow on permeability (specimen unconfined except 60-psi vertical loading). More-rapid pressure loss indicates higher permeability. (b) Effect of repeated high-pressure LN flow on permeability (under confining stresses). (c) Effect of specimen temperature on permeability (under confining stresses).

Acoustic results before breakdown tests generally agree with the fracture profile after the breakdown tests. In particular, velocities and amplitudes significantly decreased in specimens where a major fracture was identified (**Figs. 14 and 15,** Locations 5 through 10). Because waves interrogate the entire specimen, changes in wave signals (wave velocity and amplitude) reflect the average properties of the specimen; however, the effect of the locality of the sensor is significant. Signals compared with their full waveforms show that the global frequency of the signals became lower after cryogenic stimulations at nearly all measurement spots.

Changes in *P*-wave velocities are summarized in **Fig. 16.** Lower velocities near the edges (Nos. 1 and 8) and center (Nos. 4 and 5) show the effects of boundaries and borehole cavity. In rare cases, velocity slightly increased at a particular location, which suggests a local compressed zone. Such a signal usually takes place in the corner. These acoustic measurements suggest that they can be used to detect fractures near the borehole that are otherwise invisible to naked eyes and with X-ray computed-tomography (CT) scans.

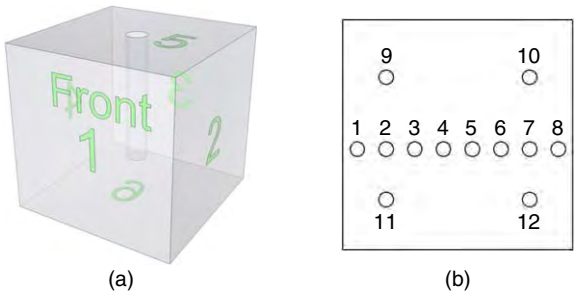

Fig. 13—Acoustic waves measured across Faces 1 and 3 and Faces 2 and 4. (a) Face-numbering convention. (b) Measurement locations on a surface.

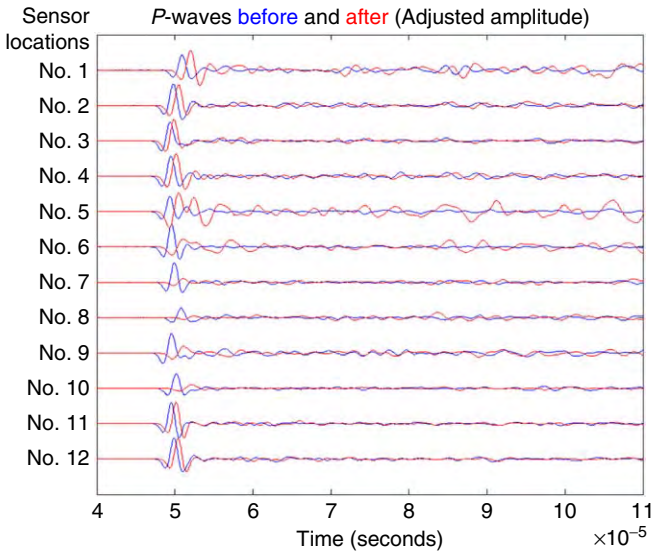

Fig. 14—*P*-wave signals (with adjusted amplitudes) across Faces 2 through 4 before and after stimulation (Specimen No. 19, Table 2).

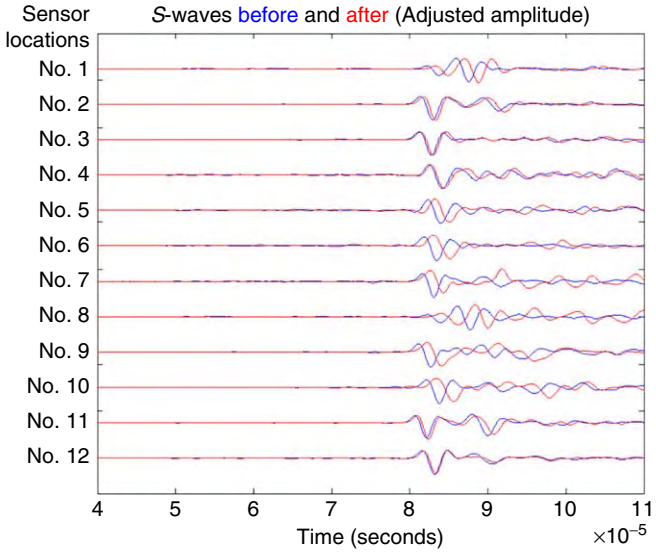

Fig. 15—*S*-wave signals (with adjusted amplitude) across Faces 2 through 4 before and after stimulation (Specimen No. 19, Table 2).

CT was attempted with a CT scanner with a voxel size $0.2\times0.2\times0.2$ mm but failed to provide enough resolution to identify cryogenically induced fractures near the wellbore. Proppants were not used in this study. Fractures created by cryogenic stimulations tended to close, as a specimen warmed. No self-propping mechanisms were observed in the laboratory-sized specimens of concrete, shale, and sandstones.

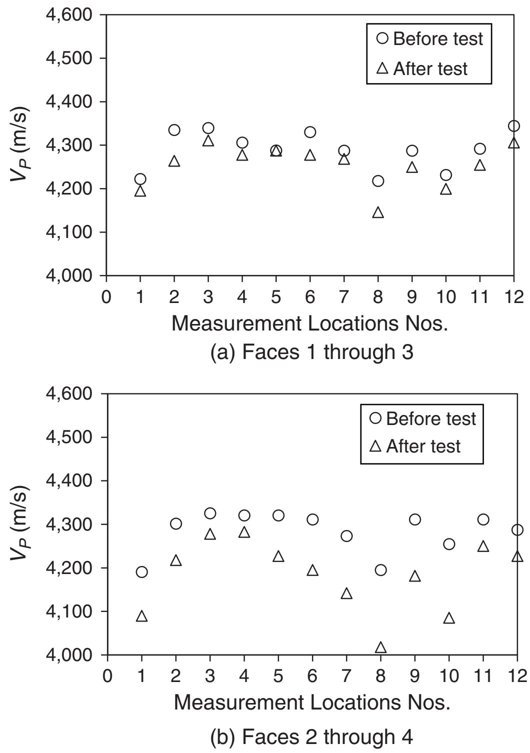

Fig. 16—*P*-wave velocity comparisons before and after treatments (Specimen No. 19, Table 2).

Breakdown Pressure and Thermal-Stress Analysis. Breakdown pressures are affected by the thermoporoelasticity of the near-wellbore formation. Coupled temperature and pore-pressure equations were solved for different formation-permeability conditions (for permeable and impermeable boundaries) under nonhydrostatic stresses (Detournay and Cheng 1988; Li et al. 1998; Chen and Ewy 2005; Wu et al. 2010). In this study, a simple estimation of expected P_{BD} for untreated specimens is performed using Eq. 1, which assumes that the breakdown occurs when the effective Terzaghi tensile stress reaches the rock tensile strength in the wall of the wellbore (Hubbert and Willis 1957; Guo et al. 1993). No initial pore pressure exists in the rock in this study, and rock is assumed impermeable. The breakdown pressure (P_{BD}) is

$$P_{BD} = 3\sigma_h - \sigma_H + \sigma_t, \quad (1)$$

where σ_H and σ_h are the maximum and minimum horizontal stresses, respectively, and σ_t is the tensile strength. The calculated P_{BD} are listed in **Table 3** and compared with the measured values.

Specimen No.	Specimen Type	Stresses (*x*:*y*:*z*) (psi)	Measured P_{BD} (psi)	Calculated P_{BD} (psi) by Eq. 1	Calculated P_{BD}– Measured P_{BD} (psi)
16	Concrete	500:750:1,000	583**	1,168	585
17	Concrete	500:750:1,000	1,180	1,168	–12
18	Concrete*	500:750:1,000	685	1,168	483
19	Concrete*	500:750:1,000	778	1,168	390
20	Concrete*	500:750:1,000	759	1,168	409
21	Concrete	1,000:1,500:2,000	1,317	1,918	601
22	Concrete*	1,000:1,500:2,000	–	1,918	–
23	Concrete*	1,000:1,500:2,000	1,094	1,918	824
S1	Shale*	1,000:1,500:2,000	1,394	2,726	1,332
S2	Shale*	1,000:3,000:4,000	1,417	1,226	–191
S4	Shale	1,000:1,500:2,000	2,439	2,726	287

*LN treated.

**Breakdown fractures concentrated near the casing.

Table 3—Comparison between measured P_{BD} and calculated P_{BD}.

During the cryogen flow through a borehole, large thermal stresses are induced by rapid cooling at the wellbore surface and near-wellbore. Estimates of the changes in the tangential thermal-stress component induced by thermal gradient on the wellbore wall are provided by Eq. 2, assuming that fractures are not created (Zoback 2010; Tarasovs and Ghassemi 2011; Zhang et al. 2014).

$$\sigma_{\max}^{\Delta T} = \frac{E}{1-\nu}\alpha \cdot \Delta T, \quad \ldots \quad (2)$$

where ΔT is temperature difference, α is the coefficient of linear thermal expansion (K^{-1}), E is static Young's modulus (psi), and ν is Poisson's ratio. From the properties in Table 1 and $\Delta T = 200°C$ that is reasonably assumed, we obtain $\sigma_{\max}^{\Delta T} = 13 \times 10^3$ psi for the concrete and 18.2×10^3 psi for the shale, which are significantly larger than the materials' tensile strengths. These indicate that fractures will occur in all cases in the absence of confining stresses.

The amount of mobilized thermal stresses required to start fractures by cooling temperature changes in a specimen under confining stress, and anisotropy relevant to this study can be estimated (Eq. 3). During the low-pressure thermal stimulations, the magnitudes of borehole pressure are negligible.

$$\sigma_{\text{mobilized}}^{\Delta T} = 3\sigma_h - \sigma_H + \sigma_t. \quad \ldots \quad (3)$$

For $\sigma_h = 1{,}000$ psi and $\sigma_H = 1{,}500$ psi, the thermal stresses mobilized to start fractures are $\sigma_{\text{mobilized}}^{\Delta T} = 1{,}920$ psi for the concrete and 2,730 psi for the shale, which are far less than the $\sigma_{\max}^{\Delta T}$ estimated previously.

Concrete Specimen No. 17 was fractured by GN pressure without LN treatment. The measured P_{BD} of the specimen is close to the calculated P_{BD} using Eq. 1, which does not consider thermal effects (Table 3). The P_{BD} for Specimen No. 17 can, therefore, be used as a baseline P_{BD} for the other tests using concrete specimens. Table 3 shows that Concrete Specimens Nos. 18 through 20, which were treated with LN with different procedures, have lower P_{BD} values than that of Specimen No. 17 and that calculated from Eq. 1. The P_{BD} of Specimen No. 18 was reduced by 42%, whereas Specimens Nos. 19 and 20 were reduced by approximately 36%. Note that Specimen No. 18 was stimulated by low-pressure LN flow for 30 minutes under low pressure, which may be a more-substantial stimulation than single-cycle high-pressure LN flow that was applied to Specimens Nos. 19 and 20. Concrete Specimens Nos. 21 through 23 were tested under higher triaxial loadings than Nos. 16 through 20. Specimen No. 23 was treated, and its P_{BD} value was lower by 43% than the calculated P_{BD}. The P_{BD} for Specimen No. 21 (untreated) is higher than the P_{BD} of Specimen No. 23, but found to be lower than the calculated P_{BD} by 31%. Some possibilities of the difference between the P_{BD} of the untreated specimen and the calculated may include damages during the higher loading and inhomogeneities in the concrete created during fabrication.

Shale Specimens Nos. S1 and S4 were tested under the same triaxial loading as Concrete Specimens Nos. 21 through 23. S1 was treated with LN and shows a P_{BD} reduced by 43% compared with the P_{BD} for S4, which was not treated with LN. Shale Specimen No. S2 was tested under the high-stress anisotropy, making its calculated P_{BD} low because of the high maximum horizontal stress σ_H (Eq. 1). Standing as an exception, the measured P_{BD} for Shale Specimen No. S2 is found to be slightly higher than the calculated P_{BD}. Other than that case, LN treatments all reduced the P_{BD} needed to start the fracture.

Discussion

Laboratory Tests and Field Delivery of LN. Boundary and scale effects are inherent in laboratory-sized specimens. Our specimen size (8 in.) is limited by the capacity and dimension of the triaxial frame to apply reservoir-level stresses, and small 1-in.-diameter central wellbores were chosen to maintain sufficient thermal gradient and generate thermal stress as fractures begin and propagate. The fracture traces observed in Cha et al. (2016a) using transparent specimens with a similar size show that a set of radial and vertical thermal fractures were created and propagate outward because of locally developed thermal stresses. As the fractures approach boundaries, however, the fracture-growth rate tended to slow down. Tarasovs and Ghassemi (2014) revealed similar quasiuniform distances between fractures, and self-similarity and scaling of thermal-shock fractures. Haimson and Zhao (1991) and Ito et al. (1990) showed that P_{BD} tends to decrease with increasing wellbore diameter, and laboratory tests in boreholes greater than 20 mm in diameter yield P_{BD} essentially unaffected by borehole diameters and are usable in interpretation of field data.

Significant amounts of LN may be needed per stimulation in the field. In this study, up to 25 L of LN was consumed for low-pressure flow of LN through 1-in. wellbore for 30 minutes. In the field, assuming a wellbore of 5-in. inner diameter and 5-hour low-pressure flow in an open borehole and considering the cross-sectional area and similar flow rate, the volume 6250 L or 1650 gal may be estimated. However, heat loss caused by long delivery to wells and longer isolated zones will significantly increase this figure depending on site characteristics and stimulation schemes. On the other hand, LN is among the cheapest cryogen, as low as USD 0.06/L, and available in large truckload quantities (Sheahen 1994; Fan 2007). LN price increases with distance from a condensing plant, and, beyond a certain distance, LN may be manufactured on-site and will still be relatively inexpensive (Fan 2007).

In field applications, heat loss and integrity of transport lines and casing may be issues to overcome for delivery of LN to the downhole environment. For both vertical and horizontal wells, the injection pipe string should have minimum contact with the casing so as not to affect casing integrity and to minimize heat loss. The injection pipes should maintain sufficient strength and structural integrity at cryogenic temperature. Suitable materials include stainless steel, brass, and fiberglass (Wilson et al. 1995). Fiberglass has the merit of a lower cost, lighter weight, and lower thermal conductivity, and for these reasons was tried in field tests (McDaniel et al. 1997). Because of inherent heat loss, the delivery pipe should be cooled before the cryogen can flow in a liquid state. From our laboratory experience, faster flow rate helps overall thermal flux, reducing the relative rate of heat loss. Nevertheless, heat loss is inevitable and may increase at greater depth.

Comparisons With Thermal Stresses During Hydraulic Fracturing. In hydraulic fracturing using water, thermal effects from injection of a cold fracturing fluid further stimulate the hydraulic fractures. The temperature difference between injected water and downhole formation of oil/gas wells at typical depth is 20 to 60°C (but can be much greater for an enhanced geothermal field), considerably less than the range of 200–250°C at cryogenic fracturing. In addition, in water fracturing, water is injected under pressure rather than flowing through. As water flows in the propagated fractures and/or permeates into the formation, thermal equilibrium with the formation could be reached quickly (Salimzadeh et al. 2016). Nevertheless, intensive cooling indeed accelerates the propagation of fractures when fluid pressure imposed is fixed. The increased fracture aperture by the thermal effect also reduces the friction loss and allows fluid pressure to reach fracture tips more effectively (Wu et al. 2016). However, in water fracturing, pressure still dominates the fracturing process, whereas the thermal stresses induced by the temperature differences plays only an assisting role. The hydraulic/thermal coupled load during injection of cool water may substantially reduce Earth stresses around injection wells, causing them to fracture at pressures considerably lower than would be expected in the absence of the thermoelastic effect (Perkins and Gonzalez 1985; Wu et al. 2016). Compared with cool water, LN can start purely thermal fractures with little or no additional pressure.

Hydraulic fractures tend to grow normal to the minimum horizontal stress. Injection of cold fracturing water into reservoir rock induces thermal cracks perpendicular to hydraulic fracture, creating a jointed fracture system. The heat transfer cools down the zone

neighboring the fracture and the rock shrinks in the direction parallel to the extension of hydraulic fractures (Perkins and Gonzalez 1985; Enayatpour and Patzek 2013). Numerical studies show growth of multiple thermal cracks during hydraulic fracturing improves the productivity; thermal cracks in rock have the potential to improve the productivity of wells in tight formations by 20% (Enayatpour and Patzek 2013). During hydraulic fracturing, thermally induced stress may open cemented natural fractures. Despite the small sizes of these fractures, their large numbers may increase the formation-contact area significantly (Dahi Taleghani et al. 2014).

Influence of Fracturing-Fluid Properties. The rheology of fracturing fluid has a strong influence on the creation and propagation of the fractures (Bohloli and de Pater 2006). Slickwater treatments use low-viscosity fluids pumped at high rates to generate narrow, complex fractures with low concentrations of propping agent (King 2010). For conventional bowing fractures, the fracturing fluid must be sufficiently viscous to transport higher proppant concentrations. These treatments are often pumped at lower pump rates and may create wider fractures. When a lower-viscosity fluid is used, the fluid infiltrates into the fracture more readily. Crack-starting pressure and breakdown pressure for the low-viscosity fluid are lower than those for high-viscosity fluid (Shimizu et al. 2011; Zhang et al. 2017). Increasing the viscosity of the fracture fluid decreases the local extent of the propagation of the microseismic cloud (Hosseini et al. 2014).

Unlike pressure-based fracturing, the fractures created during the low-pressure cryogenic flow are purely caused by thermal shock. In this case, thermal properties of the cryogen gain importance because they affect heat transfer **(Table 4).** The viscosity of nitrogen at various temperatures affects the rate at which injected nitrogen leaks through the created fractures (Table 4). Under the higher-pressure cryogenic-flow situation, where borehole pressure is used to aid fracture creation and propagation, rheology of LN and GN will be relevant. The difference in fracture generation and propagation between high-viscosity and low-viscosity fluids, as has been previously discussed in the literature (Hosseini et al. 2014), may be used as a guide to project the performance of LN and GN but verification such as microseismic will be needed. In this study, we tried to use GN to break the specimens after they were treated by LN. In the field, a similar procedure may be used to use GN after a thermal stimulation to propagate the fractures.

	Water*	GN*	LN**
Viscosity (cp)	1.002	1.76×10^{-2}	0.158
Density (g/cm^3)	0.998	0.0012	0.807
Surface tension (dynes/cm) (against air)	72.8	–	8.85
Specific heat [kJ/(kg·K)]	4.18	1.04	2.04
Thermal conductivity [W/(m·K)]	0.591	0.025	0.140

*Normal temperature and pressure (20°C and 1 atm).
**77K and 1 atm.

Table 4—Some properties of injection fluids.

Fracturing by GN has already demonstrated success in reservoirs found sensitive to liquid (Freeman et al. 1983). In the Ohio Shale Formation, GN fracturing, even without proppants, outperformed conventional stimulation systems (Abel 1981). Nitrogen is inert, and problems of clay swelling, clay migration, or oil/water emulsions are eliminated (Gottschling and Royce 1985). Cost is normally less than conventional hydraulic fracturing, and also less expensive than other gases (Clancy and Gilchrist 1983; Gottschling and Royce 1985). Yet, width reductions in unpropped fractures typically occur in the early stage of production. The viscosities of GN and LN are 1/50 and 1/6.3 of that of water, respectively (Table 4). Clearly, they imply low proppant-carrying ability. However, either high velocity injection (Gottschling and Royce 1985; Gupta and Bobier 1998) or ultralight and/or small proppants may be used with LN and GN.

Conclusions

Cryogenic fracturing was investigated as a well-stimulation technique. An integrated experimental system was designed for the first controlled laboratory cryogenic-fracturing study at wellbore conditions under true triaxial loading. We conducted cryogenic-fracturing tests using laboratory rock blocks and found that fractures are clearly generated by LN flow through a borehole under low and high flow pressure. The effectiveness of cryogenic-fracturing processes depends on cryogen-flow pressure/rate, treatment time and cycles, rock properties, and triaxial-loading conditions.

Cryogenically driven fractures were started from the borehole surfaces and propagated adjacent to the boreholes to some extent, indicating that borehole pressurization may be needed to induce deeper fracture penetration. However, P_{BD} levels are significantly lowered by cryogenic stimulation. This reduction of P_{BD} levels is possible by the formation of seed fractures created during cryogenic stimulation in the borehole. The cryogenic-stimulation schemes applied in this study are capable of reducing the P_{BD} values of concrete and shale blocks by approximately 40%.

In cryogenically stimulated specimens, the direction of fracture propagation upon applying breakdown-fracture pressure can deviate from the directions theoretically expected in specimens under triaxial-stress anisotropy. Apparently, cryogenic stimulations alter local stress fields around the wellbore, and could lead to tortuous fractures. High-stress anisotropy, however, may suppress the isotropic cryogenic thermal stress and result in the conventionally expected direction of breakdown fractures—perpendicular to the minimum-stress direction.

The profiles of borehole pressure decay obtained before and after each stage of stimulation show that low- and high-pressure LN flows increase the permeability of treated specimens. Multiple treatments in shale blocks demonstrate that increasing the number of stimulations increases permeability possibly by furthering fracture propagation and creating new fractures. We also observed the effect of temperature at the time of measurements. As temperature returns to ambient, the cryogenically generated fractures tend to close, resulting in permeability reduction. Acoustic measurements confirm that LN stimulations generate microfractures inside the blocks, which will increase the matrix permeability.

The understanding obtained in this study may be further developed for field-scale applications. The cryogenic-fracturing technique might reduce water usage and minimize the formation damage. It could also be used in combination with other conventional stimulation technologies. In particular, when applied before another pressure-based treatment, it can effectively reduce the P_{BD} by creating seed fractures.

Nomenclature

P_{BD} = breakdown pressure, psi
q = gas-flow rate, scf/D
T_o = tensile strength, psi
μ = gas viscosity, cp
σ_{avg} = average in-situ stresses, psi
σ_h = minimum horizontal stress, psi
σ_H = maximum horizontal stress, psi

Acknowledgments

Support for this research was provided by the Research Partnership to Secure Energy for America (RPSEA) (Grant No.10122-20). This work was also supported by Foundation CMG. Author T. J. Kneafsey performed work at Lawrence Berkeley National Laboratory of the US Department of Energy under Contract No. DE-AC02-05CH11231 with funding provided by RPSEA through the Ultra-Deepwater and Unconventional Natural Gas and Other Petroleum Resources Program authorized by the US Energy Policy Act of 2005. RPSEA is a nonprofit corporation whose mission is to provide a stewardship role in ensuring the focused research, development, and deployment of safe and environmentally responsible technology that can effectively deliver hydrocarbons from US resources to the citizens of the US. RPSEA, operating as a consortium of premier US energy research universities, industry, and independent research organizations, manages the program under a contract with the Department of Energy's National Energy Technology Laboratory.

References

Abel, J. C. 1981. Application of Nitrogen Fracturing in the Ohio Shale. Presented at the SPE Eastern Regional Meeting, Columbus, Ohio, 4–6 November. SPE-10378-MS. https://doi.org/10.2118/10378-MS.

Alqatahni, N. B., Cha, M., Yao, B. et al. 2016. Experimental Investigation of Cryogenic Fracturing of Rock Specimens Under True Triaxial-Confining Stresses. Presented at SPE Europec featured at 78th EAGE Conference and Exhibition, Vienna, Austria, 30 May–2 June. SPE-180071-MS. https://doi.org/10.2118/180071-MS.

ASTM D3967-16, Standard Test Method for Splitting Tensile Strength of Intact Rock Core Specimens. 2008. Conshohocken, Pennsylvania: ASTM International.

ASTM C192/C192M-16a, Standard Practice for Making and Curing Concrete Test Specimens in the Laboratory. 2014a. Conshohocken, Pennsylvania: ASTM International.

ASTM D7012-14e1, Standard Test Methods for Compressive Strength and Elastic Moduli of Intact Rock Core Specimens Under Varying States of Stress and Temperatures. 2014b. Conshohocken, Pennsylvania: ASTM International.

Beugelsdijk, L. J. L., de Pater, C. J., and Sato, K. 2000. Experimental Hydraulic Fracture Propagation in a Multi-Fractured Medium. Presented at the SPE Asia Pacific Conference on Integrated Modelling for Asset Management, Yokohama, Japan, 25–26 April. SPE-59419-MS. https://doi.org/10.2118/59419-MS.

Bohloli, B. and de Pater, C. J. 2006. Experimental Study on Hydraulic Fracturing of Soft Rocks: Influence of Fluid Rheology and Confining Stress. *J. Pet. Sci. Eng.* **53** (1–2): 1–12. https://doi.org/10.1016/j.petrol.2006.01.009.

Cha, M. and Cho, G. C. 2007. Compression Wave Velocity of Cylindrical Rock Specimens: Engineering Modulus Interpretation. *Japan. J. Appl. Phys.* **46** (1): 4497–4499. https://doi.org/10.1143/JJAP.46.4497.

Cha, M., Alqahtani, N., Yao, B. et al. 2016a. Studying Cryogenic Fracturing Process Using Transparent Specimens. *Proc.,* 1st International Conference on Energy Geotechnics, Kiel, Germany, 29–31 August, 211–216.

Cha, M., Alqahtani, N. B., Yao, B. et al. 2016b. Development of Laboratory System for Cryogenic Fracturing Study. *Proc.,* 1st International Conference on Energy Geotechnics, Kiel, Germany, 29–31 August, 381–388.

Cha, M., Alqahtani, N. B., Yin, X. et al. 2017. Laboratory System for Studying Cryogenic Thermal Rock Fracturing for Well Stimulation. *J. Pet. Sci. Eng.* **156** (July): 780–789. https://doi.org/10.1016/j.petrol.2017.06.062.

Cha, M., Cho, G. C., and Santamarina, J. C. 2009. Long-Wavelength P-Wave and S-Wave Propagation in Jointed Rock Masses. *Geophysics* **74** (5): E205–E214. https://doi.org/10.1190/1.3196240.

Cha, M., Yin, X., Kneafsey, T. et al. 2014. Cryogenic Fracturing for Reservoir Stimulation—Laboratory Studies. *J. Pet. Sci. Eng.* **124** (December): 436–450. https://doi.org/10.1016/j.petrol.2014.09.003.

Chen, G. and Ewy, R. T. 2005. Thermoporoelastic Effect on Wellbore Stability. *SPE J.* **10** (2): 121–129. SPE-89039-PA. https://doi.org/10.2118/89039-PA.

Clancy, J. P. and Gilchrist, R. E. 1983. Nitrogen Injection Applications Emerge in the Rockies. Presented at the SPE Rocky Mountain Regional Meeting, Salt Lake City, Utah, 22–25 May. SPE-11848-MS. https://doi.org/10.2118/11848-MS.

Dahi Taleghani, A., Ahmadi, M., Wang, W. et al. 2014. Thermal Reactivation of Microfractures and its Potential Impact on Hydraulic-Fracture Efficiency. *SPE J.* **19** (5): 761–770. SPE-163872-PA. https://doi.org/10.2118/163872-PA.

Detournay, E. and Carbonell, R. 1997. Fracture-Mechanics Analysis of the Breakdown Process in Minifracture or Leakoff Test. *SPE Prod & Fac* **12** (3): 195–199. SPE-28076-PA. https://doi.org/10.2118/28076-PA.

Detournay, E. and Cheng, A.-D. 1988. Poroelastic Response of a Borehole in a Non-Hydrostatic Stress Field. *Int. J. Rock Mech. Min.* **25** (3): 171–182. https://doi.org/10.1016/0148-9062(88)92299-1.

Enayatpour, S. and Patzek, T. 2013. Thermal Shock in Reservoir Rock Enhances the Hydraulic. Presented at the Unconventional Resources Technology Conference, Denver, 12–14 August. URTEC-1620617-MS.

Fan, K. 2007. Price of Liquid Nitrogen. The Physics Factbook, www.hypertextbook.com/facts/2007/KarenFan.shtml (accessed 30 January 2018).

Fenghour, A., Wakeham, W. A., and Vesovic, V. 1998. The Viscosity of Carbon Dioxide. *J. Phys. Chem. Ref. Data* **27** (1): 31–44. https://doi.org/10.1063/1.556013.

Freeman, E. R., Abel, J. C., Kim, C. M. et al. 1983. A Stimulation Technique Using Only Nitrogen. *J Pet Technol* **35** (12): 2165–2174. SPE-10129-PA. https://doi.org/10.2118/10129-PA.

Gottschling, J. C. and Royce, T. N. 1985. Nitrogen Gas and Sand: A New Technique for Stimulation of Devonian Shale. *J Pet Technol* **37** (5): 901–907. SPE-12313-PA. https://doi.org/10.2118/12313-PA.

Grundmann, S. R., Rodvelt, G. D., Dials, G. A. et al. 1998. Cryogenic Nitrogen as a Hydraulic Fracturing Fluid in the Devonian Shale. Presented at the SPE Eastern Regional Meeting, Pittsburgh, Pennsylvania, 9–11 November. SPE-51067-MS. https://doi.org/10.2118/51067-MS.

Guo, F., Morgenstern, N. R., and Scott, J. D. 1993. Interpretation of Hydraulic Fracturing Breakdown Pressure. *Int. J. Rock Mech. Min.* **30** (6): 617–626. https://doi.org/10.1016/0148-9062(93)91221-4.

Guo, T., Zhang, S., Qu, Z. et al. 2014. Experimental Study of Hydraulic Fracturing for Shale by Stimulated Reservoir Volume. *Fuel* **128** (15 July): 373–380. https://doi.org/10.1016/j.fuel.2014.03.029.

Gupta, D. V. S. and Bobier, D. M. 1998. The History and Success of Liquid CO_2 and CO_2/N_2 Fracturing System. Presented at the SPE Gas Technology Symposium, Calgary, 15–18 March. SPE-40016-MS. https://doi.org/10.2118/40016-MS.

Haimson, B. C. and Zhao, Z. 1991. Effect of Borehole Size and Pressurization Rate on Hydraulic Fracturing Breakdown Pressure. Presented at the 32nd US Symposium on Rock Mechanics (USRMS), Norman, Oklahoma, 10–12 July. ARMA-91-191.

Hosseini, S. M., Neuhaus, C. W., and Aminzadeh, F. 2014. Effect of Fluid Rheology and Reservoir Compressibility on Microseismicity During Hydraulic Fracturing. Presented at the SPE Annual Technical Conference and Exhibition, Amsterdam, 27–29 October. SPE-170897-MS. https://doi.org/10.2118/170897-MS.

Hubbert, M. K. and Willis, D. G. 1957. Mechanics of Hydraulic Fracturing. SPE-686-G.

Ito, T., Hayashi, K., and Abe, H. 1990. Scale Effect in Breakdown Pressure of Hydraulic Fracturing Stress Measurements. *Proc.,* Scale Effects in Rock Masses: Proceedings of the First International Workshop on Scale Effects in Rock Masses, Loen, Norway, 7–8 June, 289–295. Rotterdam, The Netherlands: AA Balkema.

Kendrick, D., Puskar, M., and Schlotterbeck, S. T. 2005. Ultralightweight Proppants: A Field Study in the Big Sandy Field of Eastern Kentucky. Presented at the SPE Eastern Regional Meeting, Morgantown, West Virginia, 14–16 September. SPE-98006-MS. https://doi.org/10.2118/98006-MS.

King, G. E. 2010. Thirty Years of Gas Shale Fracturing: What Have We Learned? Presented at the SPE Annual Technical Conference and Exhibition, Florence, Italy, 19–22 September. SPE-133456-MS. https://doi.org/10.2118/133456-MS.

King, S. R. 1983. Liquid CO_2 for the Stimulation of Low-Permeability Reservoirs. Presented at the SPE/DOE Low Permeability Gas Reservoirs Symposium, Denver, 14–16 March. SPE-11616-MS. https://doi.org/10.2118/11616-MS.

Lecampion, B., Desroches, J., Jeffrey, R. et al. 2016. Experiments versus Theory for the Initiation and Propagation of Radial Hydraulic Fractures in Low Permeability Materials. *J. Geophys. Res.-Sol. Ea.* **122** (2): 1239–1263. https://doi.org/10.1002/2016JB013183.

Lhomme, T., Detournay, E., and Jeffrey, R. 2005. Effect of Fluid Compressibility and Borehole Radius on the Propagation of a Fluid-Driven Fracture. Oral presentation given at the 11th International Conference on Fracture, Turin, Italy, 20–25 March.

Li, X., Cui, L., and Roegiers, J.-C. 1998. Thermoporoelastic Modelling of Wellbore Stability in Non-Hydrostatic Stress Field. *Int. J. Rock Mech. Min.* **35** (4–5): 584. https://doi.org/10.1016/S0148-9062(98)00079-5.

Lillies, A. T. and King, S. R. 1982. Sand Fracturing with Liquid Carbon Dioxide. Presented at the SPE Production Technology Symposium, Hobbs, New Mexico, 8–9 November. SPE-11341-MS. https://doi.org/10.2118/11341-MS.

Mazza, R. L. 1997. Liquid CO_2 Improves Fracturing. *Hart's Oil and Gas World*, Vol. 22. Houston: Hart Publications.

McDaniel, B. W., Grundmann, S. R., Kendrick, W. D. et al. 1997. Field Applications of Cryogenic Nitrogen as a Hydraulic Fracturing Fluid. Presented at the SPE Annual Technical Conference and Exhibition, San Antonio, Texas, 5–8 October. SPE-38623-MS. https://doi.org/10.2118/38623-MS.

Nicot, J.-P. and Scanlon, B. R. 2012. Water Use for Shale-Gas Production in Texas, US. *Environ. Sci. Technol.* **46** (6): 3580–3586. https://doi.org/10.1021/es204602t.

Perkins, T. and Gonzalez, J. 1985. The Effect of Thermoelastic Stresses on Injection Well Fracturing. *SPE J.* **25** (1): 78–88. SPE-11332-PA. https://doi.org/10.2118/11332-PA.

Rudenko, N. S. and Schubnikow, L. W. 1968. The Viscosity of Liquid Nitrogen, Carbon Monoxide, Argon and Oxygen as a Function of Temperature. Report NASA-TT-F-11-868.

Salimzadeh, S., Paluszny, A., and Zimmerman, R. 2016. Thermal Effects During Hydraulic Fracturing in Low-Permeability Brittle Rocks. Presented at the 50th US Rock Mechanics/Geomechanics Symposium, Houston, 26–29 June. ARMA-2016-368.

Shaefer, M. T. 2005. Are Slick Water-Fracturing Applications Effective in the J-Sand Formation? Presented at the SPE Annual Technical Conference and Exhibition, Dallas, 9–12 October. SPE-96933-MS. https://doi.org/10.2118/96933-MS.

Sharma, M. M., Gadde, P. B., Sullivan, R. et al. 2004. Slick Water and Hybrid Fracs in the Bossier: Some Lessons Learnt. Presented at the SPE Annual Technical Conference and Exhibition, Houston, 26–29 September. SPE-89876-MS. https://doi.org/10.2118/89876-MS.

Sheahen, T. 1994. *Introduction to High-Temperature Superconductivity*. New York City: Springer Science & Business Media.

Shimizu, H., Murata, S., and Ishida, T. 2011. The Distinct Element Analysis for Hydraulic Fracturing in Hard Rock Considering Fluid Viscosity and Particle Size Distribution. *Int. J. Rock Mech. Min.* **48** (5): 712–727. https://doi.org/10.1016/j.ijrmms.2011.04.013.

Steward, D. B. 2013. George P. Mitchell and the Barnett Shale. *J Pet Technol* **65** (11): 58–68. SPE-1113-0058-JPT. https://doi.org/10.2118/1113-0058-JPT.

Tarasovs, S. and Ghassemi, A. 2011. Propagation of a System of Cracks Under Thermal Stress. Presented at the 45th US Rock Mechanics/Geomechanics Symposium, San Francisco, 26–29 June. ARMA-11-558.

Tarasovs, S. and Ghassemi, A. 2014. Self-Similarity and Scaling of Thermal Shock Fractures. *Phys. Rev. E* **90** (1): 012403. https://doi.org/10.1103/PhysRevE.90.012403.

Wang, L., Yao, B., Cha, M. et al. 2016. Waterless Fracturing Technologies for Unconventional Reservoirs-Opportunities for Liquid Nitrogen. *J. Nat. Gas Sci. Eng.* **35** (A): 160–174. https://doi.org/10.1016%2Fj.jngse.2016.08.052.

Wilson, D. R., Siebert, R. M., and Lively, P. 1995. Cryogenic Coal Bed Gas Well Stimulation Method. US Patent No. 5,464,061.

Wu, B., Zhang, X., and Jeffrey, R. 2010. A Thermo-Poro-Elastic Analysis of Stress Fields Around a Borehole. Presented at the 44th US Rock Mechanics Symposium and 5th US-Canada Rock Mechanics Symposium, Salt Lake City, Utah, 27–30 June. ARMA-10-442.

Wu, B., Zhang, X., and Jeffrey, R. G. 2016. Analysis of Thermal Effects on Hydraulic Fracturing Near a Horizontal Well by Using Displacement Discontinuity Method. Presented at the SPE Asia Pacific Hydraulic Fracturing Conference, Beijing, 24–26 August. SPE-181865-MS. https://doi.org/10.2118/181865-MS.

Zhang, X., Jeffrey, R. G., and Wu, B. 2014. Crack Propagation From a Surface Assisted by Fluid Pressure and Cooling. Presented at the 48th US Rock Mechanics/Geomechanics Symposium, Minneapolis, Minnesota, 1–4 June. ARMA-2014-6995.

Zhang, X., Lu, Y., Tang, J. et al. 2017. Experimental Study on Fracture Initiation and Propagation in Shale Using Supercritical Carbon Dioxide Fracturing. *Fuel* **190** (15 February): 370–378. https://doi.org/10.1016/j.fuel.2016.10.120.

Zoback, M. D. 2010. *Reservoir Geomechanics*. Cambridge, UK: Cambridge University Press.

SI Metric Conversion Factors

in. × 2.54*	E−02 = m
g/cm^3 × 1.0	E+03 = kg/m^3
md × 1.01325	E+12 = m^2
psi × 1.45038	E−04 = Pa
(°F−32)/1.8	= °C

*Conversion factor is exact.

Minsu Cha is an assistant professor in the Zachry Department of Civil Engineering at Texas A&M University. Previously, he was a post-doctoral fellow in the Petroleum Engineering Department and the Civil Engineering Department at the Colorado School of Mines. Cha's research interests lie in the study of fundamental concepts and engineering solutions that address geochallenges related to energy geoengineering, such as sediment dissolution, reservoir geomechanics, CO_2 geostorage, and geothermal energy. He has authored or coauthored more than 20 technical papers. Cha holds PhD and master's degrees in geotechnical engineering from the Georgia Institute of Technology; a master's degree in civil engineering from KAIST, Korea; and a bachelor's degree from Pusan National University, Korea. He is a member of SPE.

Naif B. Alqahtani is an assistant research professor in the National Center for Oil and Gas Technology at King Abdulaziz City for Science and Technology, Saudi Arabia, where he has worked for more than 11 years. His current interests are stimulations, hydraulic fracturing, well completions, artificial lift, rock mechanics, and unconventional reservoirs. Alqahtani has authored or coauthored more than nine technical publications since 2010. He holds a bachelor's degree in petroleum engineering from King Saud University, Saudi Arabia, and master's and PhD degrees in petroleum engineering from the Colorado School of Mines.

Bowen Yao is a PhD degree student in petroleum engineering. He has participated in the RPSEA project of Development of Non-Contaminating Cryogenic Fracturing Technology for Shale and Tight Gas Reservoirs. Yao is currently working on the project of Quantitative Characterization of Impacts of Coupled Geomechanics and Flow on Safe and Permanent Geological Storage of CO_2 in Fractured Aquifers. His main research focus is on the experiments and simulation of the rock-fracturing process coupled with geomechanics and thermal effect. Yao holds a bachelor's degree in mechanical engineering from Shanghai Jiao Tong University, China, and a master's degree in petroleum engineering from the Colorado School of Mines.

Xiaolong Yin is an associate professor in the Petroleum Engineering Department at the Colorado School of Mines. His research interests cover computational fluid dynamics, phase behavior of petroleum fluids, and suspensions and flows through porous media. Yin has authored or coauthored more than 75 technical publications since 2005. He holds a bachelor's degree in theoretical and applied mechanics from Peking University, China; a master's degree in mechanical engineering from Lehigh University; and a PhD degree in chemical engineering from Cornell University. Yin is an associate editor for *SPE Journal* and a member of the SPE Reservoir Description and Dynamics Advisory Committee.

Timothy Kneafsey is a professional engineer and a geological staff scientist at Lawrence Berkeley National Laboratory. Over the past 25 years, he has worked on and led laboratory and field studies investigating thermal, hydrological, mechanical, and chemical processes affecting heat and mass transfer in fractured and porous rock relevant to geothermal-energy production, CO_2 sequestration, hydrocarbon production from gas and oil shales, gas production from methane-hydrate-bearing sediments, and radioactive-waste disposal. Kneafsey has authored or coauthored more than 45 peer-reviewed journal articles and holds one US patent. He holds bachelor's degrees in mechanical and civil engineering from the University of New Mexico, and master's and PhD degrees in civil and environmental engineering from the University of California at Berkeley.

Lei Wang is a post-doctoral-degree researcher in the Petroleum Engineering Department at the Colorado School of Mines. His research interests include cryogenic fracturing, CO_2 sequestration, fluid flow and phase change in nanoporous media, and enhanced-oil-recovery (EOR) processes. Wang has authored or coauthored more than 20 technical papers. He holds a bachelor's degree in environmental engineering, a master's degree in petroleum engineering from China University of Petroleum (East China), and a PhD degree in petroleum engineering from the Colorado School of Mines.

Yu-Shu Wu is a professor, Foundation CMG Reservoir Modeling Chair, and director of the Energy Modeling Group (EMG) Research Center in the Petroleum Engineering Department at the Colorado School of Mines, where he teaches and performs research in reservoir engineering, multiphase-fluid and heat flow, geomechanics, unconventional-oil/gas-reservoir dynamics, CO_2 geosequestration and EOR, geothermal engineering, and numerical-reservoir simulation. Wu leads the EMG in its research effort in flow dynamics in unconventional oil and gas reservoirs; coupled processes of multiphase fluid and heat flow, geomechanics, and chemical transport in porous and fractured media; CO_2 sequestration and EOR application; improved formation-stimulation/cryogenic-fracturing technologies; and advanced reservoir-simulation technologies. Previously, he was a staff scientist with the Earth Sciences Division of the Lawrence Berkeley National Laboratory for 14 years from 1995 to 2008. During his career, Wu has authored or coauthored more than 120 peer-reviewed journal papers and 17 peer-reviewed books/chapters as well as 62 SPE papers. He is a fellow of the Geological Society of America and a Distinguished Member of SPE.

Jennifer L. Miskimins is the associate department head and an associate professor in the Petroleum Engineering Department at the Colorado School of Mines. Her research interests focus in the areas of hydraulic fracturing, stimulation, completions, and unconventional reservoirs. Miskimins has authored or coauthored more than 75 technical papers. She holds a bachelor's degree in petroleum engineering from the Montana College of Mineral Science and Technology, and master's and PhD degrees in petroleum engineering from the Colorado School of Mines. Miskimins served as an SPE Distinguished Lecturer during the 2010–2011 and 2013–2014 seasons, was the executive editor of *SPE Production & Operations* from 2008–2011, and was the recipient of the 2014 SPE International Completions Optimization and Technology Award.